Acta Cryst E
CRYSTALLOGRAPHIC COMMUNICATIONS
ISSN 2056-9890

[(*Z*)-*N*-(3-Fluorophenyl)-*O*-methylthiocarbamato-*κS*](triphenylphosphane-*κP*)gold(I): crystal structure, Hirshfeld surface analysis and computational study

Chien Ing Yeo, Sang Loon Tan, Huey Chong Kwong and Edward R. T. Tiekink*

Research Centre for Crystalline Materials, School of Science and Technology, Sunway University, 47500 Bandar Sunway, Selangor Darul Ehsan, Malaysia. *Correspondence e-mail: edwardt@sunway.edu.my

Received 9 July 2020
Accepted 10 July 2020

Edited by W. T. A. Harrison, University of Aberdeen, Scotland

Keywords: crystal structure; gold; thiocarbamate; Hirshfeld surface analysis; computational chemistry.

CCDC reference: 2015568

Supporting information: this article has supporting information at journals.iucr.org/e

The title phosphanegold(I) thiolate, $C_{26}H_{22}AuFNOPS$ or [Au(C_8H_7FNOS)($C_{18}H_{15}P$)], has the Au^I centre coordinated by phosphane-P [2.2494 (8) Å] and thiolate-S [2.3007 (8) Å] atoms to define a close to linear geometry [P—Au—S = 176.10 (3)°]. The thiolate ligand is orientated so that the methoxy-O atom is directed towards the Au atom, forming an Au···O close contact of 2.986 (2) Å. In the crystal, a variety of intermolecular contacts are discerned with fluorobenzene-C—H···O(methoxy) and phenyl-C—H···F interactions leading to dimeric aggregates. These are assembled into a three-dimensional architecture by phenyl-C—H···S(thiolate) and phenyl-C—H···π(fluorobenzene, phenyl) interactions. Accordingly, the analysis of the calculated Hirshfeld surface shows 30.8% of all contacts are of the type C···H/H···C but this is less than the H···H contacts, at 44.9%. Other significant contributions to the surface come from H···F/F···H [8.1%], H···S/S···H [6.9%] and H···O/O···H [3.2%] contacts. Two major stabilization energies have contributions from the phenyl-C—H···π(fluorobenzene) and fluorobenzene-C—H···C(imine) interactions (−37.2 kcal mol^{-1}), and from the fluorobenzene-C—H···F and phenyl-C—H···O interactions (−34.9 kcal mol^{-1}), the latter leading to the dimeric aggregate.

1. Chemical context

In common with many other phosphanegold(I) thiolates (Yeo *et al.*, 2018), molecules of the general formula R_3PAu[SC(OR')═NAr] have proven to exhibit anti-cancer potential (Ooi *et al.*, 2017). Complimenting this activity is anti-bacterial potential against Gram-positive bacteria based on *in vitro* assays and time-kill profiles (Yeo *et al.*, 2013) but not anti-amoebic effects, *i.e.* against *Acanthamoeba castellanii* (Siddiqui *et al.*, 2017). In keeping with suggestions that the incorporation of fluorine atoms into molecules can enhance their pharmaceutical utility (Müller *et al.*, 2007; Meanwell, 2018), it was thought of interest to synthesize fluoro analogues of R_3PAu[SC(OR')═NAr].

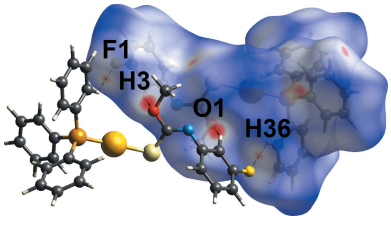

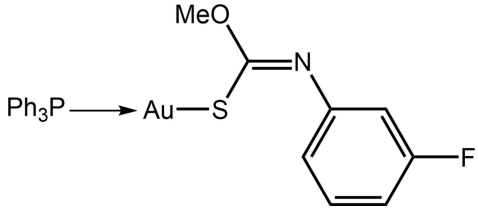

Herein, the compound with R = Ph, R' = Me and Ar = 3-fluorobenzene, (I), is described: synthesis, spectroscopic

OPEN ACCESS

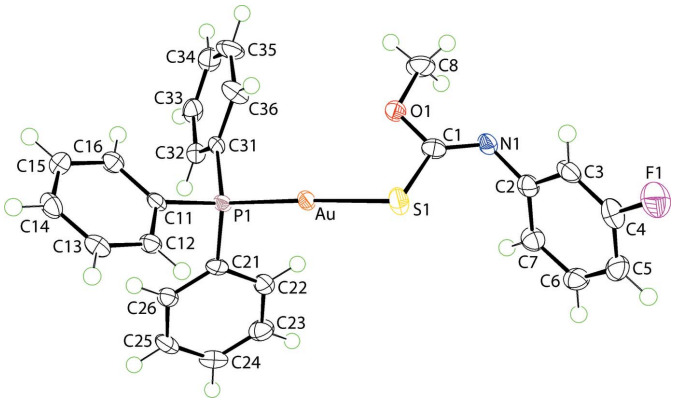

Figure 1
The molecular structures of (I) showing the atom-labelling scheme and displacement ellipsoids at the 70% probability level.

characterization, crystal structure determination, analysis of the calculated Hirshfeld surfaces and interaction energies.

2. Structural commentary

The molecular structure of (I), Fig. 1, features a linearly coordinated Au^{I} centre defined by phosphane-P1 [2.2494 (8) Å] and thiolate-S1 [2.3007 (8) Å] atoms. The deviation of the P1—Au—S1 angle of 176.10 (3)° from the ideal 180° is related to the close approach of the O1 atom, *i.e.* Au···O1 = 2.986 (2) Å, as the O1 atom is directed towards the gold atom. The elongation of the C1—S1 bond to 1.762 (3) Å and the shortening of the C1—N1 bond to 1.262 (4) Å with respect to the comparable bonds in the neutral thiocarbamide molecules, *i.e.* S═C(OMe)N(H)Ar (Ho *et al.*, 2005), *i.e. ca* 1.66 and 1.34 Å, respectively, are consistent with the formation of thiolate and imine bonds, respectively.

The overall molecular conformation of (I) is as usually found in molecules formulated as R_3PAu[SC(O*R*′)═NAr]. However, a less common form is known whereby the N-bound aryl ring is orientated towards the gold atom rather than the alkoxy-oxygen atom (Kuan *et al.*, 2008). So, rather than an intramolecular Au···O contact, an intramolecular Au···π contact is formed. The observation of both forms in Ph_3PAu[SC(OEt)═NPh], *i.e.* with Au···O (Hall & Tiekink, 1993) or Au···π (Yeo *et al.*, 2016), suggests the energy difference between the conformations is relatively small. In related binuclear species, DFT calculations suggest that a Au···π interaction is about 6 kcal mol^{-1} more stable than a Au···O contact (Yeo *et al.*, 2015).

3. Supramolecular features

Several directional intermolecular points of contact between molecules are noted in the extended structure of (I); see Table 1 for a listing of the geometric parameters characterizing these. Centrosymmetrically related molecules are connected *via* pairwise fluorobenzene-C—H···O1 and phenyl-C—H···F1 contacts Fig. 2(*a*). The dimeric aggregates are connected into a three-dimensional architecture by phenyl-C—H···S1 interactions, with the phenyl-H atom involved in the latter interaction, *i.e.* H13, also participating in a C—H···π(fluorobenzene) interaction and so may be considered bifurcated. The two remaining contacts are of the type phenyl-C—H···π(fluorobenzene, phenyl) so the fluorobenzene ring accepts two contacts, one to either side of the ring. A view of the unit-cell contents is shown in Fig. 2(*b*).

Table 1
Hydrogen-bond geometry (Å, °).

*Cg*1 and *Cg*2 are the centroids of the (C2–C7) and (C11–C16) rings, respectively.

D—H···*A*	*D*—H	H···*A*	*D*···*A*	*D*—H···*A*
C3—H3···O1^{i}	0.95	2.42	3.269 (3)	148
C36—H36···F1^{i}	0.95	2.51	3.218 (4)	131
C13—H13···S1^{ii}	0.95	2.83	3.519 (3)	130
C13—H13···*Cg*1^{ii}	0.95	2.74	3.500 (3)	137
C22—H22···*Cg*1^{iii}	0.95	2.63	3.397 (3)	138
C24—H24···*Cg*2^{iv}	0.95	2.80	3.552 (3)	137

Symmetry codes: (i) $-x+1, -y+1, -z+1$; (ii) $-x+\frac{1}{2}, y-\frac{1}{2}, -z+\frac{1}{2}$; (iii) $-x, -y+1, -z+1$; (iv) $x-1, y, z$.

4. Hirshfeld surface analysis

In order to understand further the interactions operating in the molecular packing of (I), the Hirshfeld surfaces mapped over normalized contact distance d_{norm} (McKinnon *et al.*, 2004) and two-dimensional fingerprint plots (Spackman & McKinnon, 2002) for (I) were generated using *Crystal*

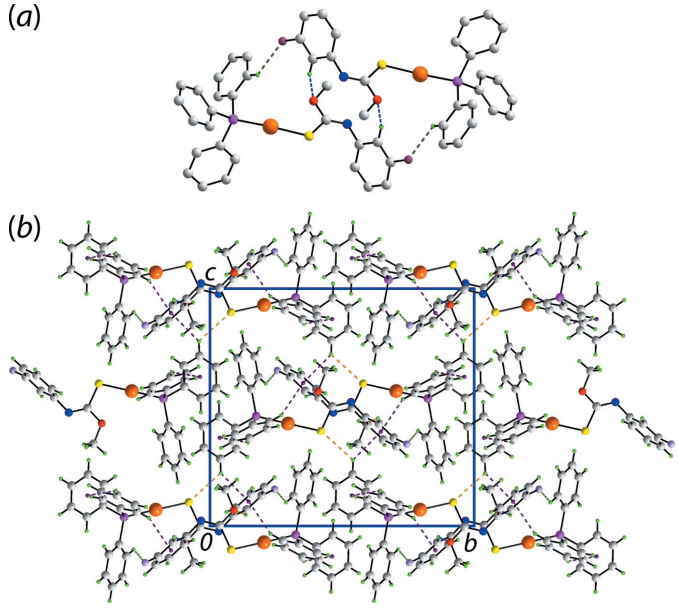

Figure 2
Molecular packing in the crystal of (I): (*a*) the two-molecule aggregate sustained by fluorobenzene-C—H···O and phenyl-C—H···F contacts shown as blue and green dashed lines, respectively (non-participating H atoms are omitted) and (*b*) a view of the unit-cell contents down the *a* axis with phenyl-C—H···S and phenyl-C—H···π(fluorobenzene, phenyl) interactions shown as orange and purple dashed lines, respectively.

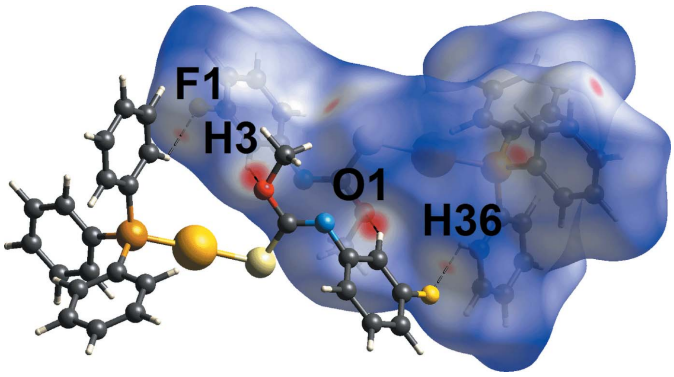

Figure 3
Views of the Hirshfeld surface for (I) mapped over d_{norm} in the range −0.222 to +1.382 arbitrary units, highlighting C—H···O/F interactions.

Explorer 17 (Turner *et al.*, 2017) following literature procedures (Tan *et al.*, 2019). The bright-red spots near the fluorobenzene-H3 and methoxy-O1 atoms on the Hirshfeld surface mapped over d_{norm} in Fig. 3, correspond to the fluorobenzene-C3—H3···O1 contacts. These contacts are associated with phenyl-C36—H36···F1 contacts, which appear as faint red spots in Fig. 3, being ~0.24 Å shorter than the respective sums of their van der Waals radii, Table 2. The phenyl-C13—H13···S1 interaction is observed as faint red spots on the d_{norm} surface in Fig. 4(*a*), where the cooperative phenyl-C13—H13···π(C2–C7) interaction is shown as a distinctive orange 'pothole' on the shape-index-mapped Hirshfeld surface in Fig. 4(*b*). Although the phenyl-C22—H22···π(C2–C7) interaction was not manifested on the Hirshfeld surface mapped over d_{norm}, this interaction shows up as blue 'bump' and orange 'pothole' near the H22 atom and *Cg*1(C2–C7) centroid, respectively, in Fig. 5(*a*). Simultaneously, a fluorobenzene-C7—H7···C1(imine) contact, Table 2, is observed through faint red spots near atoms C1 and H7 on the d_{norm} surface in Fig. 5(*b*). The presence of the phenyl-C24—H24···π(C11–C16) contact is evidenced through faint red spots in Fig. 6(*a*) and the orange 'pothole' in Fig. 6(*b*) on the d_{norm} and shape-index mapped Hirshfeld surface, respectively. In addition to the C—H···π contacts listed in Table 1, weak phenyl-C32—H32···π(C11–C16) and phenyl-C15—H15···π(C21–C26) contacts, Table 2, are observed as an orange 'hollow' on the Hirshfeld surface mapped over shape-index property in Fig. 7.

Table 2
A summary of short interatomic contacts (Å) for (I)[a].

Contact	Distance	Symmetry operation
C3—H3···O1[b]	2.31	$-x+1, -y+1, -z+1$
C36—H36···F1[b]	2.43	$-x+1, -y+1, -z+1$
C13—H13···S1[b]	2.74	$-x+\frac{1}{2}, y-\frac{1}{2}, -z+\frac{1}{2}$
C7—H7···C1	2.66	$-x, -y+1, -z+1$
H8*C*···H33	2.31	$-x+\frac{1}{2}, y+\frac{1}{2}, -z+\frac{3}{2}$
C15—H15···*Cg*(C21–C26)	3.23	$-x, -y, -z+1$
C32—H32···*Cg*(C11–C16)	3.22	$-x, -y, -z+1$

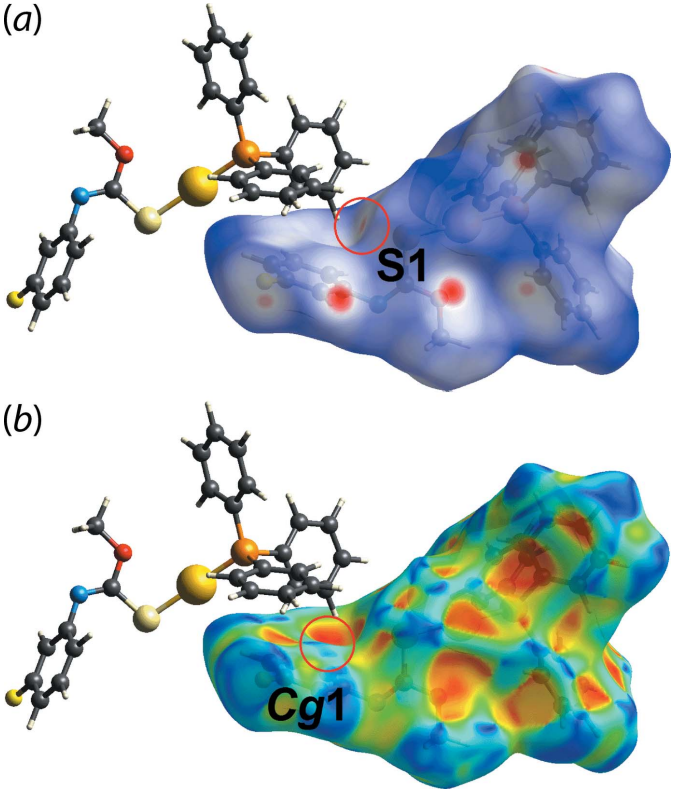

Figure 4
Views of the Hirshfeld surface mapped for (I) over (*a*) d_{norm} in the range of −0.222 to +1.382 arbitrary units and (*b*) the shape-index property. The C—H···S and C—H···π interaction are highlighted within red circles.

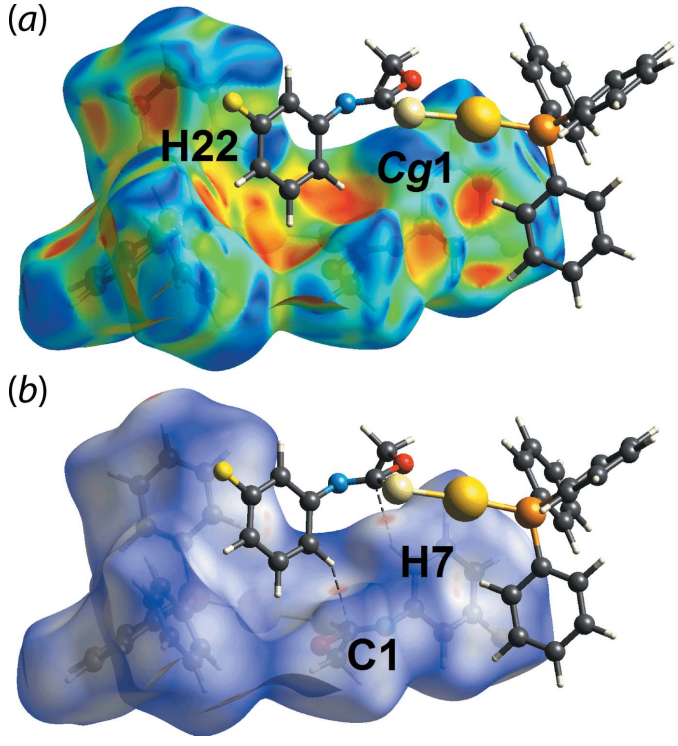

Figure 5
Views of the Hirshfeld surface mapped for (I) over (*a*) the shape-index property and (*b*) d_{norm} in the range of −0.222 to +1.382 arbitrary units.

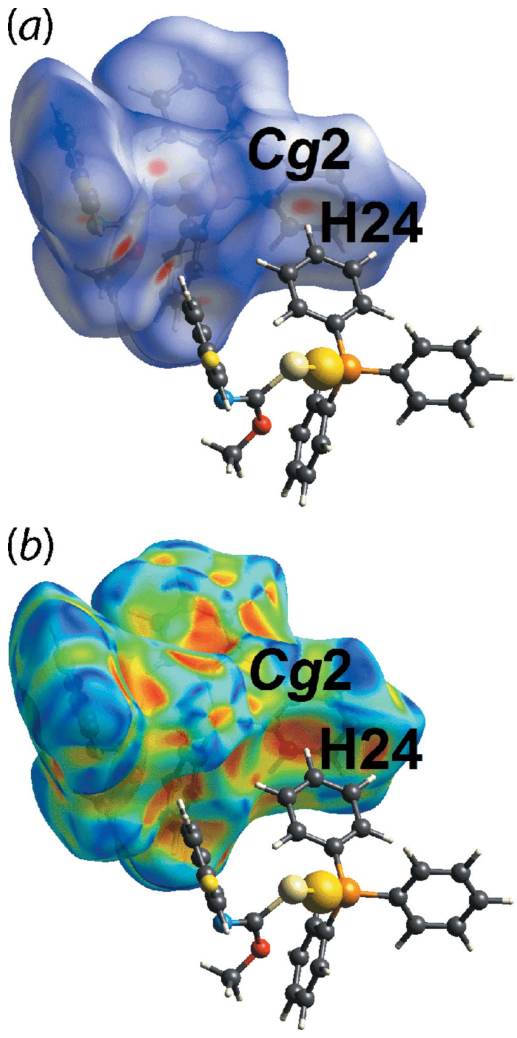

Figure 6
Views of the Hirshfeld surface mapped for (I) over (*a*) d_{norm} in the range of −0.222 to +1.382 arbitrary units and (*b*) the shape-index property, each highlighting the phenyl-C24—H24···π(C11–C16) interaction.

The overall two-dimensional fingerprint plot of (I) is shown in Fig. 8(*a*), and those delineated into H···H, H···C/C···H, H···F/F···H, H···S/S···H and H···O/O···H contacts are shown in Fig. 8(*b*)–(*f*), respectively. The percentage contributions for the different interatomic contacts to the Hirshfeld surface are summarized in Table 3. The H···H contacts are the most prominent of all contacts and contribute 44.9% to the entire surface. The delineated fingerprint plot in Fig. 8(*b*) features a beak-shaped peak tipped at $d_e + d_i$ ~2.3 Å. This tip corresponds to a methyl-H8*C*···H33(phenyl) contact and has a distance 0.1 Å shorter than the sum of their van de Waals radii, Table 2. Consistent with the many C—H···π interactions evident in the molecular packing, H···C/C···H contacts contribute 30.8% to the total surface contacts. The H···C/C···H contacts shows a distinctive feature in the fingerprint plot of Fig. 8(*c*) with two symmetric spikes at $d_e + d_i$ ~2.4 Å. The tips of pseudo-mirrored sharp spikes at $d_e + d_i$ ~2.4 Å represent the shortest H···F/F···H contacts (8.1%), Fig. 8(*d*),

Table 3
Percentage contributions of interatomic contacts to the Hirshfeld surface for (I).

Contact	Percentage contribution
H···H	44.9
H···C/C···H	30.8
H···F/F···H	8.1
H···S/S···H	6.9
H···O/O···H	3.2
Others	6.1

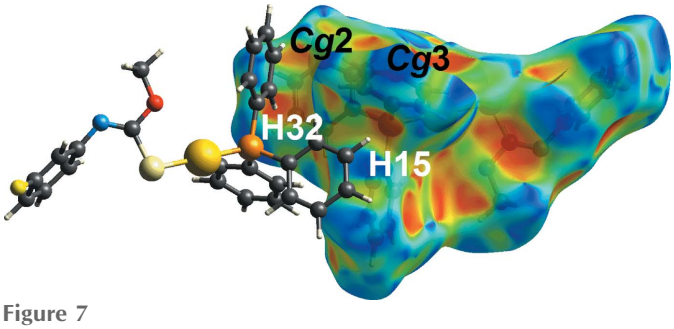

Figure 7
A view of the Hirshfeld surface mapped for (I) over the shape-index property highlighting weak C15—H15···π(C21–C26) and C32—H32···π(C11–C16) interactions.

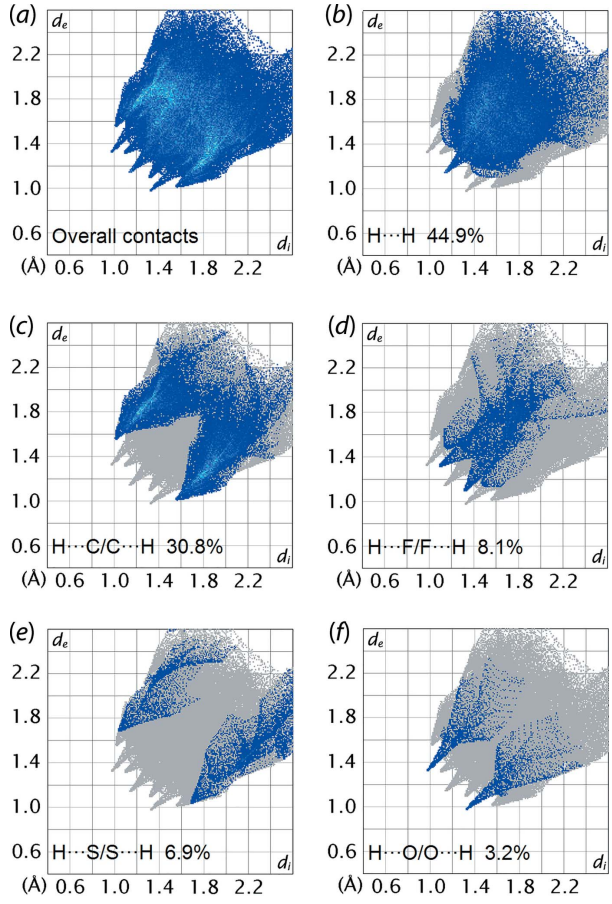

Figure 8
(*a*) The overall two-dimensional fingerprint plots for (I), and those delineated into (*b*) H···O/O···H, (*c*) H···C/C···H, (*d*) H···F/F···H, (*e*) H···S/S···H and (*f*) H···O/O···H contacts, with the percentage contributions specified within each plot.

Table 4
A summary of interaction energies (kcal mol^{-1}) calculated for (I).

Contact	E_{int}^{BSSE}	Symmetry operation
C22—H22···π(C2–C7) (×2) + C7—H7···C1 (×2)	−37.2	$-x, -y+1, -z+1$
C36—H36···F1 (×2) + C3—H3···O1 (×2)	−34.9	$-x+1, -y+1, -z+1$
C32—H32···π(C11–C16) (×2) + C15—H15···π(C21–C26) (×2)	−15.6	$-x, -y, -z+1$
C13—H13···π(C2–C7) + C13—H13···S1	−8.9	$-x+\frac{1}{2}, y-\frac{1}{2}, -z+\frac{1}{2}$
C24—H24···π(C11–C16)	−5.4	$x-1, y, z$

and correspond to the phenyl-C36—H36···F1 contact in Table 1. While the C—H···O1 and C—H···S1 interactions are reflected through two sharp-symmetric wings at $d_e + d_i$ ~2.7 and ~2.5 Å, respectively, Fig. 8(*e*) and (*f*), these types of contacts only contribute 6.9 and 3.2%, respectively, to the total interatomic contacts. The accumulated contribution of the remaining six different interatomic contacts is around 6.0% and these do not have a significant influence on the molecular packing.

5. Computational chemistry

The interaction energies in the crystal of (I) were calculated based on the procedures reported previously (Yusof *et al.*, 2017). Briefly, the corresponding pairwise molecules were subjected to the calculation *via* the long-range corrected ωB97XD functional combining the D2 version of Grimme's dispersion model (Chai & Head-Gordon, 2008), with Pople's 6-31+G(d,p) basis set (Petersson *et al.*, 1988; Petersson & Al-Laham, 1991) comprising the polarization and diffuse functions being employed for C, H, N, O, F, P and S while the effective core potential LANL2DZ (Hay & Wadt, 1985) was applied for Au. Counterpoise methods (Boys & Bernardi, 1970; Simon *et al.*, 1996) were applied to correct for basis set superposition error (BSSE) in the obtained energies. The BSSE corrected interaction energies (*E*) are listed in Table 4.

The greatest stabilization energy arises from the phenyl-C22—H22···π(C2–C7) and fluorobenzene-C7—H7···C1(imine) interactions (−37.2 kcal mol^{-1}). This is followed by the phenyl-C36—H36···F1 and phenyl-C3—H3···O1 interactions (−34.9 kcal mol^{-1}), which lead to the dimeric aggregate in Fig. 2(*a*). The other directional contacts outlined in *Supramolecular features* contribute minor stabilization energies to the molecular packing (−8.9 + −5.46 kcal mol^{-1}) while the pairwise weak phenyl-C15—H15···π(C21–C26) and phenyl-C32—H32···π(C11–C16) interactions, which were identified through the *Hirshfeld surface analysis*, have a greater stabilization energy (−15.6 kcal mol^{-1}).

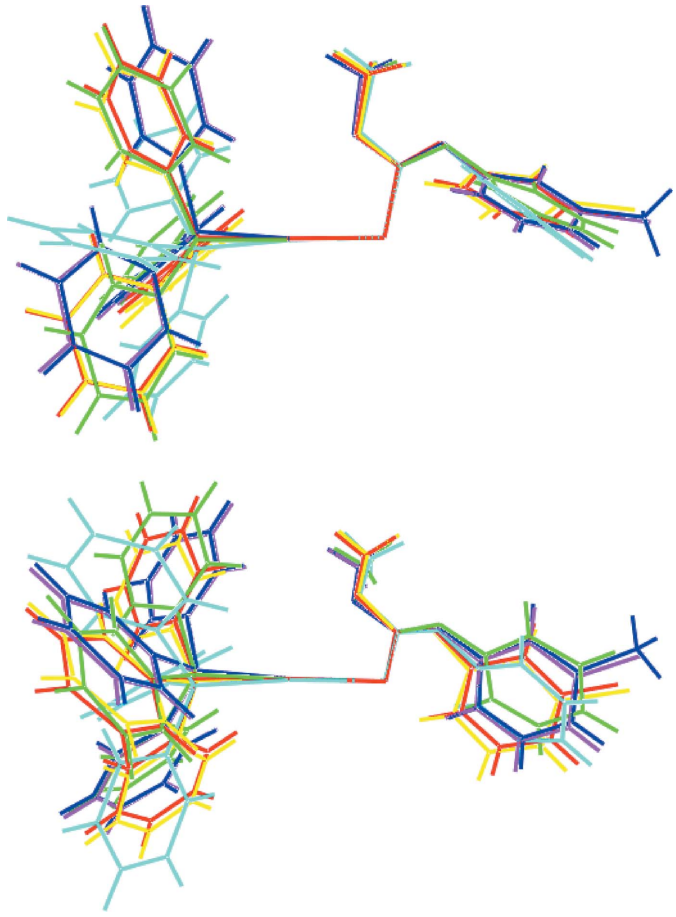

Figure 9
Overlay diagram for (I) (red image) and $Ph_3PAu[SC(OMe){=}NC_6H_4Y\text{-}3]$ for *Y* = H (green), H (chloroform solvate, aqua), Me (blue), Cl (triclinic form, pink) and Cl (monoclinic form, yellow). The molecules have been overlapped so the Au, S1 and C1 atoms are coincident.

6. Database survey

There are several literature precedents for (I), *i.e.* molecules of the general formula $Ph_3PAu[SC(OMe){=}NC_6H_4Y\text{-}3]$. Selected geometric parameters for these are given in Table 5. To a first

Table 5
A summary of key geometric parameters (Å, °) for structures related to (I).

Y	Au—S	Au—P	P—Au—S	Au···O	CNOS/C_6	REFCODE	Ref.
H	2.3005 (14)	2.2578 (12)	177.72 (4)	3.045 (4)	87.18 (18)	HADZAN	Hall & Tiekink (1993)
H[a]	2.3102 (14)	2.2613 (12)	175.96 (5)	3.140 (3)	78.4 (2)	COCRUI	Kuan *et al.* (2008)
Me	2.2968 (15)	2.2479 (11)	175.12 (4)	2.954 (3)	74.69 (16)	COCROC	Kuan *et al.* (2008)
Cl[b]	2.2903 (17)	2.2416 (14)	174.61 (5)	2.988 (3)	75.01 (14)	VUYKOQ	Tadbuppa & Tiekink (2010)
Cl[c]	2.3071 (15)	2.2535 (15)	175.62 (5)	3.052 (3)	73.95 (16)	VUYKOQ01	Yeo *et al.* (2016)
F	2.3007 (8)	2.2494 (8)	176.10 (3)	2.986 (2)	78.73 (9)	–	This work

Notes: (*a*) chloroform solvate; (*b*) $P\bar{1}$ polymorph; (*c*) $P2_1/c$ polymorph.

approximation, the molecules adopt similar conformations and each features a short intramolecular Au···O interaction. This being stated, the two overlay diagrams in Fig. 9 indicate differences in the relative dispositions of the terminal arene rings, as reflected in the differences in the dihedral angles between the planes through the CNOS and C_6 residues, which vary by up to nearly 15°. Finally, there is an isostructural relationship between (I) and the monoclinic form of the Y = Cl compound (Yeo *et al.*, 2016).

7. Synthesis and crystallization

All chemicals and solvents were used as sourced without further purification. Melting points were determined on a Biobase automatic melting point apparatus MP450 (Jinan, Shandong Province, China). ^{1}H and ^{13}C{^{1}H} NMR spectra were recorded in $CDCl_3$ solution on a Bruker Ascend 400 MHz NMR spectrometer (Billerica, MA, USA) with chemical shifts relative to tetramethylsilane; the ^{31}P{^{1}H} NMR spectrum was recorded in $CDCl_3$ solution on the same instrument but with the chemical shift recorded relative to 85% aqueous H_3PO_4 as the external reference. IR spectra were measured on a Bruker Vertex 70v FTIR spectrophotometer (Billerica, MA, USA) from 4000 to 400 cm^{-1}. Elemental analyses were performed on a Leco TruSpec MicroCHN Elemental Analyser (St Joseph, MI, USA).

The thiol precursor, LH, was prepared from the reaction of 3-fluorophenyl isothiocyanate (Sigma–Aldrich, St. Louis, MO, USA; 2.50 mmol, 0.38 g) and MeOH (Merck, Kenilworth, NJ, USA; 100 ml) in the presence of NaOH (Merck, Kenilworth, NJ, USA; 2.50 mmol, 0.10 g) followed by the addition of excess 1 *M* HCl. The resulting mixture was extracted using chloroform, yielding colourless crystals after 3 weeks standing. Yield: 0.421 g (91%), m.p. 334.0–334.5 K. Analysis calculated for C_8H_8FNOS: C, 51.88; H, 4.35; N, 7.56%. Found: C, 51.49; H, 4.46; N, 7.42%. IR (cm^{-1}): 3241 (*br*) ν(N—H), 1438 (*s*) ν(C—N), 1150 (*s*) ν(C—O), 1048 (*s*) ν (C═S). ^{1}H NMR (400 MHz, $CDCl_3$, 298 K): δ 8.88 (*s*, *br*, 1H, NH), 7.29–6.87 (*m*, 4H, aryl-H), 4.15 (*s*, 3H, OCH_3) ppm. ^{13}C{^{1}H} NMR (400 MHz, $CDCl_3$, 298 K): δ 189.4 (Cq), 162.8 (*d*, aryl-C_3, $^1J_{CF}$ = 245.80 Hz), 138.5 (aryl-C_1), 130.2 (*d*, aryl-C_5, $^3J_{CF}$ = 9.25 Hz), 116.8 (aryl-C_6), 112.2 (*d*, aryl-C_4, $^2J_{CF}$ = 21.25 Hz), 109.1 (aryl-C_2), 58.9 (OCH_3) ppm.

The Ph_3PAuCl precursor was prepared from the reduction of $KAuCl_4$ using sodium sulfite, followed by the addition of a stoichiometric amount of triphenylphosphane. The precipitate was used as isolated.

NaOH (Merck, Kenilworth, NJ, USA; 0.50 mmol, 0.020 g) in water (5 ml) was added to a suspension of Ph_3PAuCl (0.50 mmol, 0.247 g) in acetonitrile (20 ml), LH (0.50 mmol, 0.093 g) in acetonitrile (20 ml) was added and the solution was stirred for 3 h. The solution was left for slow evaporation at room temperature, yielding colourless crystals after 2 weeks. Yield: 0.273 g (85%), m.p. 408.0–408.5 K. Analysis calculated for $C_{26}H_{22}AuFNOPS$: C, 48.53; H, 3.45; N, 2.18%. Found: C, 48.73; H, 3.56; N, 1.97%. IR (cm^{-1}): 1575 (*s*) ν(C═N), 1122 (*s*) ν(C—O), 1100 (*s*) ν(C—S). ^{1}H NMR (400 MHz, $CDCl_3$, 298 K): δ 7.55–7.43 (*m*, *br*, 15H, Ph_3P), 6.95–6.89 (*m*, *br*, 1H, aryl-H_5), 6.63–6.61 (*m*, *br*, 2H, aryl-$H_{2,6}$), 6.39–6.36 (*m*, *br*, 1H, aryl-H_4), 3.90 (*s*, 3H, OCH_3) ppm. ^{13}C{^{1}H} NMR (400 MHz, $CDCl_3$, 298 K): δ 165.4 (Cq), 163.2 (*d*, aryl-C_3, $^1J_{CF}$ = 244.45 Hz), 152.8 (*d*, aryl-C_1, $^3J_{CF}$ = 9.93 Hz), 134.3 (*d*, 2-PC_6H_5, $^3J_{CP}$ = 13.86 Hz), 131.7 (*d*, 4-PC_6H_5, $^4J_{CP}$ = 2.30 Hz), 129.7 (*d*, aryl-C_5, $^3J_{CF}$ = 9.62 Hz), 129.3 (*d*, 3-PC_6H_5, $^1J_{CP}$ = 57.41 Hz), 129.1 (*d*, 2-PC_6H_5, $^2J_{CP}$ = 11.64 Hz), 117.8 (*d*, aryl-C_6, $^4J_{CF}$ = 2.57 Hz), 109.3 (*d*, aryl-C_2, $^2J_{CF}$ = 21.95 Hz), 109.1 (*d*, aryl-C_4, $^2J_{CF}$ = 21.27 Hz), 55.5 (OCH_3) ppm. ^{31}P{^{1}H} NMR (400 MHz, $CDCl_3$, 298 K): δ 38.8 ppm.

Table 6
Experimental details.

Crystal data	
Chemical formula	[Au(C_8H_7FNOS)($C_{18}H_{15}P$)]
M_r	643.44
Crystal system, space group	Monoclinic, $P2_1/n$
Temperature (K)	100
a, b, c (Å)	8.9311 (3), 17.2458 (6), 15.6857 (5)
β (°)	99.361 (3)
V (Å^3)	2383.80 (14)
Z	4
Radiation type	Mo $K\alpha$
μ (mm^{-1})	6.35
Crystal size (mm)	0.30 × 0.30 × 0.30
Data collection	
Diffractometer	Agilent Technologies SuperNova Dual diffractometer with Atlas detector
Absorption correction	Multi-scan (*CrysAlis PRO*; Agilent, 2013)
T_{min}, T_{max}	0.252, 1.000
No. of measured, independent and observed [$I > 2\sigma(I)$] reflections	25800, 5429, 5017
R_{int}	0.045
$(\sin \theta/\lambda)_{max}$ (Å^{-1})	0.650
Refinement	
$R[F^2 > 2\sigma(F^2)]$, $wR(F^2)$, S	0.023, 0.050, 1.08
No. of reflections	5429
No. of parameters	290
H-atom treatment	H-atom parameters constrained
$\Delta\rho_{max}$, $\Delta\rho_{min}$ (e Å^{-3})	1.17, −1.22

Computer programs: *CrysAlis PRO* (Agilent, 2013), *SHELXS97* (Sheldrick, 2015*a*), *SHELXL2018/3* (Sheldrick, 2015*b*), *ORTEP-3 for Windows* (Farrugia, 2012), *DIAMOND* (Brandenburg, 2006) and *publCIF* (Westrip, 2010).

8. Refinement

Crystal data, data collection and structure refinement details are summarized in Table 6. The carbon-bound H atoms were placed in calculated positions (C—H = 0.95–0.98 Å) and were included in the refinement in the riding-model approximation, with U_{iso}(H) set to 1.2–1.5U_{eq}(C). The maximum and minimum electron density peaks of 1.17 and 1.22 e Å^{-3}, respectively, are located 0.97 and 0.69 Å, respectively, from the Au atom.

Funding information

This research was supported by the Trans-disciplinary Research Grant Scheme (TR002-2014A) provided by the Ministry of Education, Malaysia. Sunway University Sdn Bhd

is thanked for financial support of this work through grant No. STR-RCTR-RCCM-001-2019.

References

Agilent (2013). *CrysAlis PRO*. Agilent Technologies Inc., Santa Clara, CA, USA.

Boys, S. F. & Bernardi, F. (1970). *Mol. Phys.* **19**, 553–566.

Brandenburg, K. (2006). *DIAMOND*. Crystal Impact GbR, Bonn, Germany.

Chai, J. D. & Head-Gordon, M. (2008). *Phys. Chem. Chem. Phys.* **10**, 6615–6620.

Farrugia, L. J. (2012). *J. Appl. Cryst.* **45**, 849–854.

Hall, V. J. & Tiekink, E. R. T. (1993). *Z. Kristallogr. Cryst. Mater*. **203**, 313–315.

Hay, P. J. & Wadt, W. R. (1985). *J. Chem. Phys.* **82**, 270–283.

Ho, S. Y., Bettens, R. P. A., Dakternieks, D., Duthie, A. & Tiekink, E. R. T. (2005). *CrystEngComm*, **7**, 682–689.

Kuan, F. S., Ho, S. Y., Tadbuppa, P. P. & Tiekink, E. R. T. (2008). *CrystEngComm*, **10**, 548–564.

McKinnon, J. J., Spackman, M. A. & Mitchell, A. S. (2004). *Acta Cryst.* B**60**, 627–668.

Meanwell, N. A. (2018). *J. Med. Chem.* **61**, 5822–5880.

Müller, K., Faeh, C. & Diederich, F. (2007). *Science*, **317**, 1881–1886.

Ooi, K. K., Yeo, C. I., Mahandaran, T., Ang, K. P., Akim, A. M., Cheah, Y.-K., Seng, H.-L. & Tiekink, E. R. T. (2017). *J. Inorg. Biochem.* **166**, 173–181.

Petersson, G. A. & Al-Laham, M. A. (1991). *J. Chem. Phys.* **94**, 6081–6090.

Petersson, G. A., Bennett, A., Tensfeldt, T. G., Al-Laham, M. A., Shirley, W. A. & Mantzaris, J. (1988). *J. Chem. Phys.* **89**, 2193–2218.

Sheldrick, G. M. (2015*a*). *Acta Cryst.* A**71**, 3–8.

Sheldrick, G. M. (2015*b*). *Acta Cryst.* C**71**, 3–8.

Siddiqui, R., Abjani, F., Yeo, C. I., Tiekink, E. R. T. & Khan, N. A. (2017). *J. Neg. Res. Biomed.* **16** article no. 6.

Simon, S., Duran, M. & Dannenberg, J. J. (1996). *J. Chem. Phys.* **105**, 11024–11031.

Spackman, M. A. & McKinnon, J. J. (2002). *CrystEngComm*, **4**, 378–392.

Tadbuppa, P. P. & Tiekink, E. R. T. (2010). *Acta Cryst.* E**66**, m664.

Tan, S. L., Jotani, M. M. & Tiekink, E. R. T. (2019). *Acta Cryst.* E**75**, 308–318.

Turner, M. J., McKinnon, J. J., Wolff, S. K., Grimwood, D. J., Spackman, P. R., Jayatilaka, D. & Spackman, M. A. (2017). *Crystal Explorer 17*. The University of Western Australia.

Westrip, S. P. (2010). *J. Appl. Cryst.* **43**, 920–925.

Yeo, C. I., Khoo, C.-H., Chu, W.-C., Chen, B.-J., Chu, P.-L., Sim, J.-H., Cheah, Y.-K., Ahmad, J., Halim, S. N. A., Seng, H.-L., Ng, S., Otero-de-la-Roza, A. & Tiekink, E. R. T. (2015). *RSC Adv.* **5**, 41401–41411.

Yeo, C. I., Ooi, K. K. & Tiekink, E. R. T. (2018). *Molecules*, **23**, article no. 1410.

Yeo, C. I., Sim, J.-H., Khoo, C.-H., Goh, Z.-J., Ang, K.-P., Cheah, Y.-K., Fairuz, Z. A., Halim, S. N. B. A., Ng, S. W., Seng, H.-L. & Tiekink, E. R. T. (2013). *Gold Bull.* **46**, 145–152.

Yeo, C. I., Tan, S. L., Otero-de-la-Roza, A. & Tiekink, E. R. T. (2016). *Z. Kristallogr. Cryst. Mater.* **231**, 653–661.

Yusof, E. N. M., Tahir, M. I. M., Ravoof, T. B. S. A., Tan, S. L. & Tiekink, E. R. T. (2017). *Acta Cryst.* E**73**, 543–549.

supporting information

Acta Cryst. (2020). E**76**, 1284-1290 [https://doi.org/10.1107/S2056989020009469]

[(*Z*)-*N*-(3-Fluorophenyl)-*O*-methylthiocarbamato-*κS*](triphenylphosphane-*κP*)gold(I): crystal structure, Hirshfeld surface analysis and computational study

Chien Ing Yeo, Sang Loon Tan, Huey Chong Kwong and Edward R. T. Tiekink

Computing details

Data collection: *CrysAlis PRO* (Agilent, 2013); cell refinement: *CrysAlis PRO* (Agilent, 2013); data reduction: *CrysAlis PRO* (Agilent, 2013); program(s) used to solve structure: *SHELXS97* (Sheldrick, 2015*a*); program(s) used to refine structure: *SHELXL2018/3* (Sheldrick, 2015*b*); molecular graphics: *ORTEP-3 for Windows* (Farrugia, 2012) and *DIAMOND* (Brandenburg, 2006); software used to prepare material for publication: *publCIF* (Westrip, 2010).

[(*Z*)-*N*-(3-Fluorophenyl)-*O*-methylthiocarbamato-*κS*](triphenylphosphane-*κP*)gold(I)

Crystal data

[Au(C_8H_7FNOS)($C_{18}H_{15}P$)]
M_r = 643.44
Monoclinic, $P2_1/n$
a = 8.9311 (3) Å
b = 17.2458 (6) Å
c = 15.6857 (5) Å
β = 99.361 (3)°
V = 2383.80 (14) Å^3
Z = 4
F(000) = 1248
D_x = 1.793 Mg m^{-3}
Mo $K\alpha$ radiation, λ = 0.71073 Å
Cell parameters from 12325 reflections
θ = 3.9–29.4°
μ = 6.35 mm^{-1}
T = 100 K
Block, colourless
0.30 × 0.30 × 0.30 mm

Data collection

Agilent Technologies SuperNova Dual diffractometer with Atlas detector
Radiation source: SuperNova (Mo) X-ray Source
Mirror monochromator
Detector resolution: 10.4041 pixels mm^{-1}
ω scan
Absorption correction: multi-scan (CrysAlis PRO; Agilent, 2013)
T_{min} = 0.252, T_{max} = 1.000
25800 measured reflections
5429 independent reflections
5017 reflections with $I > 2\sigma(I)$
R_{int} = 0.045
θ_{max} = 27.5°, θ_{min} = 2.8°
h = −11→11
k = −19→22
l = −20→20

Refinement

Refinement on F^2
Least-squares matrix: full
$R[F^2 > 2\sigma(F^2)]$ = 0.023
$wR(F^2)$ = 0.050
S = 1.08
5429 reflections
290 parameters
0 restraints
Primary atom site location: structure-invariant direct methods
Secondary atom site location: difference Fourier map
Hydrogen site location: inferred from neighbouring sites
H-atom parameters constrained

$w = 1/[\sigma^2(F_o^2) + (0.019P)^2 + 0.9042P]$
where $P = (F_o^2 + 2F_c^2)/3$
$(\Delta/\sigma)_{max} = 0.002$
$\Delta\rho_{max} = 1.17$ e Å^{-3}
$\Delta\rho_{min} = -1.22$ e Å^{-3}

Special details

Geometry. All esds (except the esd in the dihedral angle between two l.s. planes) are estimated using the full covariance matrix. The cell esds are taken into account individually in the estimation of esds in distances, angles and torsion angles; correlations between esds in cell parameters are only used when they are defined by crystal symmetry. An approximate (isotropic) treatment of cell esds is used for estimating esds involving l.s. planes.

Fractional atomic coordinates and isotropic or equivalent isotropic displacement parameters (Å²)

	x	*y*	*z*	U_{iso}*/U_{eq}
Au	0.19089 (2)	0.29511 (2)	0.43142 (2)	0.01422 (5)
S1	0.25242 (9)	0.42032 (5)	0.40015 (4)	0.02170 (17)
P1	0.11477 (8)	0.17558 (4)	0.46267 (4)	0.01214 (15)
F1	0.3783 (2)	0.74491 (12)	0.34520 (12)	0.0342 (5)
O1	0.3182 (2)	0.40907 (13)	0.56743 (11)	0.0174 (4)
N1	0.2716 (3)	0.53368 (14)	0.52214 (14)	0.0166 (5)
C1	0.2802 (3)	0.46274 (18)	0.50373 (17)	0.0166 (6)
C2	0.2227 (3)	0.58863 (18)	0.45714 (17)	0.0168 (6)
C3	0.3275 (3)	0.63954 (18)	0.43078 (18)	0.0196 (6)
H3	0.432629	0.635322	0.453168	0.023*
C4	0.2749 (4)	0.69595 (18)	0.3716 (2)	0.0220 (7)
C5	0.1236 (4)	0.70522 (18)	0.3365 (2)	0.0224 (7)
H5	0.091705	0.744606	0.295236	0.027*
C6	0.0213 (3)	0.65520 (19)	0.36383 (18)	0.0214 (7)
H6	−0.083664	0.660487	0.341475	0.026*
C7	0.0685 (3)	0.59706 (18)	0.42351 (18)	0.0200 (6)
H7	−0.003907	0.562999	0.441510	0.024*
C8	0.3549 (4)	0.4400 (2)	0.65366 (18)	0.0259 (7)
H8A	0.382956	0.397437	0.694599	0.039*
H8B	0.266609	0.467333	0.668620	0.039*
H8C	0.440246	0.476108	0.656412	0.039*
C11	0.2043 (3)	0.09645 (17)	0.41333 (16)	0.0137 (6)
C12	0.2005 (3)	0.09928 (18)	0.32403 (16)	0.0157 (6)
H12	0.154329	0.141957	0.291578	0.019*
C13	0.2641 (3)	0.03972 (18)	0.28306 (18)	0.0186 (6)
H13	0.261179	0.041530	0.222276	0.022*
C14	0.3322 (3)	−0.02258 (18)	0.32988 (18)	0.0197 (6)
H14	0.375062	−0.063543	0.301276	0.024*
C15	0.3376 (3)	−0.02491 (18)	0.41910 (18)	0.0198 (6)
H15	0.384366	−0.067488	0.451488	0.024*
C16	0.2747 (3)	0.03502 (18)	0.46069 (17)	0.0165 (6)
H16	0.279928	0.033867	0.521660	0.020*
C21	−0.0875 (3)	0.16265 (17)	0.42616 (16)	0.0139 (6)
C22	−0.1844 (3)	0.22366 (19)	0.43861 (18)	0.0190 (6)
H22	−0.144129	0.270054	0.465862	0.023*
C23	−0.3395 (4)	0.2166 (2)	0.4112 (2)	0.0233 (7)

H23	−0.405616	0.257836	0.420261	0.028*
C24	−0.3976 (3)	0.1491 (2)	0.37058 (18)	0.0220 (7)
H24	−0.503754	0.144248	0.351765	0.026*
C25	−0.3024 (3)	0.08884 (19)	0.35728 (17)	0.0197 (6)
H25	−0.343172	0.043087	0.328736	0.024*
C26	−0.1474 (3)	0.09489 (18)	0.38545 (16)	0.0161 (6)
H26	−0.082202	0.053035	0.377065	0.019*
C31	0.1488 (3)	0.15679 (17)	0.57834 (16)	0.0140 (6)
C32	0.0449 (3)	0.11807 (17)	0.61907 (17)	0.0177 (6)
H32	−0.047892	0.100392	0.586516	0.021*
C33	0.0759 (3)	0.10496 (18)	0.70764 (17)	0.0206 (6)
H33	0.004161	0.078454	0.735568	0.025*
C34	0.2111 (4)	0.13046 (19)	0.75517 (18)	0.0255 (7)
H34	0.232732	0.121070	0.815605	0.031*
C35	0.3144 (4)	0.1695 (2)	0.71456 (19)	0.0274 (8)
H35	0.407258	0.186851	0.747336	0.033*
C36	0.2843 (4)	0.1838 (2)	0.62661 (19)	0.0232 (7)
H36	0.355046	0.211765	0.599282	0.028*

Atomic displacement parameters (Å²)

	U^{11}	U^{22}	U^{33}	U^{12}	U^{13}	U^{23}
Au	0.01968 (7)	0.01105 (8)	0.01111 (7)	−0.00252 (4)	0.00000 (4)	−0.00008 (4)
S1	0.0393 (5)	0.0135 (4)	0.0121 (3)	−0.0044 (3)	0.0039 (3)	−0.0002 (3)
P1	0.0144 (3)	0.0121 (4)	0.0093 (3)	−0.0020 (3)	0.0002 (3)	−0.0002 (3)
F1	0.0338 (11)	0.0293 (12)	0.0403 (11)	−0.0116 (9)	0.0089 (9)	0.0050 (9)
O1	0.0231 (11)	0.0158 (12)	0.0122 (10)	0.0007 (8)	−0.0002 (8)	−0.0017 (8)
N1	0.0174 (12)	0.0141 (14)	0.0176 (12)	0.0003 (10)	0.0005 (9)	−0.0050 (10)
C1	0.0123 (13)	0.0215 (18)	0.0161 (14)	−0.0016 (12)	0.0024 (11)	−0.0005 (12)
C2	0.0187 (14)	0.0165 (17)	0.0154 (13)	0.0013 (12)	0.0029 (11)	−0.0048 (12)
C3	0.0174 (15)	0.0193 (18)	0.0208 (15)	−0.0017 (12)	−0.0001 (12)	−0.0085 (13)
C4	0.0259 (17)	0.0181 (18)	0.0239 (16)	−0.0059 (13)	0.0097 (13)	−0.0038 (13)
C5	0.0287 (18)	0.0176 (18)	0.0201 (16)	0.0058 (13)	0.0018 (13)	−0.0018 (12)
C6	0.0168 (15)	0.0229 (19)	0.0231 (15)	0.0057 (13)	−0.0009 (12)	−0.0043 (13)
C7	0.0159 (15)	0.0204 (18)	0.0238 (15)	−0.0006 (12)	0.0039 (12)	−0.0021 (13)
C8	0.0304 (18)	0.032 (2)	0.0130 (14)	0.0037 (15)	−0.0039 (12)	−0.0030 (13)
C11	0.0150 (14)	0.0132 (16)	0.0121 (12)	−0.0042 (11)	−0.0002 (10)	−0.0028 (11)
C12	0.0176 (14)	0.0169 (17)	0.0119 (13)	−0.0014 (12)	0.0000 (10)	−0.0010 (11)
C13	0.0193 (15)	0.0225 (18)	0.0137 (13)	−0.0038 (12)	0.0022 (11)	−0.0046 (12)
C14	0.0171 (15)	0.0193 (18)	0.0233 (15)	−0.0007 (12)	0.0050 (12)	−0.0091 (13)
C15	0.0202 (15)	0.0161 (17)	0.0219 (15)	0.0021 (12)	−0.0002 (12)	0.0015 (12)
C16	0.0182 (14)	0.0179 (17)	0.0135 (13)	−0.0018 (12)	0.0026 (11)	−0.0013 (12)
C21	0.0155 (14)	0.0192 (17)	0.0068 (12)	−0.0026 (11)	0.0013 (10)	0.0020 (11)
C22	0.0192 (15)	0.0182 (17)	0.0186 (15)	0.0017 (12)	−0.0002 (12)	−0.0039 (12)
C23	0.0192 (15)	0.027 (2)	0.0227 (15)	0.0059 (13)	0.0008 (12)	−0.0003 (14)
C24	0.0157 (15)	0.034 (2)	0.0151 (14)	−0.0024 (13)	−0.0010 (11)	0.0014 (13)
C25	0.0227 (16)	0.0212 (18)	0.0141 (14)	−0.0094 (13)	−0.0007 (11)	−0.0019 (12)
C26	0.0174 (14)	0.0169 (17)	0.0135 (13)	−0.0018 (12)	0.0007 (11)	0.0000 (12)

C31	0.0186 (14)	0.0114 (16)	0.0111 (13)	0.0008 (11)	−0.0006 (10)	−0.0028 (11)
C32	0.0202 (15)	0.0146 (16)	0.0175 (14)	0.0008 (12)	0.0006 (11)	−0.0005 (12)
C33	0.0312 (17)	0.0159 (17)	0.0153 (14)	−0.0003 (13)	0.0051 (12)	0.0028 (12)
C34	0.042 (2)	0.0215 (19)	0.0117 (14)	0.0042 (15)	−0.0012 (13)	0.0003 (13)
C35	0.0310 (18)	0.031 (2)	0.0163 (15)	−0.0063 (15)	−0.0088 (13)	−0.0016 (14)
C36	0.0239 (16)	0.0272 (19)	0.0181 (15)	−0.0089 (14)	0.0017 (12)	−0.0048 (14)

Geometric parameters (Å, º)

Au—P1	2.2494 (8)	C13—H13	0.9500
Au—S1	2.3007 (8)	C14—C15	1.393 (4)
S1—C1	1.762 (3)	C14—H14	0.9500
P1—C11	1.817 (3)	C15—C16	1.389 (4)
P1—C21	1.818 (3)	C15—H15	0.9500
P1—C31	1.819 (3)	C16—H16	0.9500
F1—C4	1.365 (3)	C21—C26	1.396 (4)
O1—C1	1.364 (3)	C21—C22	1.396 (4)
O1—C8	1.441 (3)	C22—C23	1.387 (4)
N1—C1	1.262 (4)	C22—H22	0.9500
N1—C2	1.408 (4)	C23—C24	1.387 (5)
C2—C3	1.394 (4)	C23—H23	0.9500
C2—C7	1.400 (4)	C24—C25	1.379 (4)
C3—C4	1.374 (4)	C24—H24	0.9500
C3—H3	0.9500	C25—C26	1.387 (4)
C4—C5	1.382 (4)	C25—H25	0.9500
C5—C6	1.375 (4)	C26—H26	0.9500
C5—H5	0.9500	C31—C32	1.382 (4)
C6—C7	1.390 (4)	C31—C36	1.399 (4)
C6—H6	0.9500	C32—C33	1.390 (4)
C7—H7	0.9500	C32—H32	0.9500
C8—H8A	0.9800	C33—C34	1.384 (4)
C8—H8B	0.9800	C33—H33	0.9500
C8—H8C	0.9800	C34—C35	1.379 (5)
C11—C16	1.385 (4)	C34—H34	0.9500
C11—C12	1.397 (4)	C35—C36	1.384 (4)
C12—C13	1.382 (4)	C35—H35	0.9500
C12—H12	0.9500	C36—H36	0.9500
C13—C14	1.385 (4)		
P1—Au—S1	176.10 (3)	C13—C14—C15	119.7 (3)
C1—S1—Au	101.30 (10)	C13—C14—H14	120.1
C11—P1—C21	104.91 (13)	C15—C14—H14	120.1
C11—P1—C31	106.09 (13)	C16—C15—C14	120.0 (3)
C21—P1—C31	106.78 (12)	C16—C15—H15	120.0
C11—P1—Au	115.21 (9)	C14—C15—H15	120.0
C21—P1—Au	111.34 (10)	C11—C16—C15	120.0 (2)
C31—P1—Au	111.91 (10)	C11—C16—H16	120.0
C1—O1—C8	115.4 (2)	C15—C16—H16	120.0

C1—N1—C2	120.6 (2)	C26—C21—C22	119.7 (3)
N1—C1—O1	120.5 (2)	C26—C21—P1	122.3 (2)
N1—C1—S1	127.5 (2)	C22—C21—P1	118.1 (2)
O1—C1—S1	112.0 (2)	C23—C22—C21	120.1 (3)
C3—C2—C7	119.3 (3)	C23—C22—H22	120.0
C3—C2—N1	119.6 (3)	C21—C22—H22	120.0
C7—C2—N1	120.8 (3)	C22—C23—C24	119.7 (3)
C4—C3—C2	118.3 (3)	C22—C23—H23	120.1
C4—C3—H3	120.9	C24—C23—H23	120.1
C2—C3—H3	120.9	C25—C24—C23	120.5 (3)
F1—C4—C3	118.0 (3)	C25—C24—H24	119.7
F1—C4—C5	118.3 (3)	C23—C24—H24	119.7
C3—C4—C5	123.7 (3)	C24—C25—C26	120.2 (3)
C6—C5—C4	117.4 (3)	C24—C25—H25	119.9
C6—C5—H5	121.3	C26—C25—H25	119.9
C4—C5—H5	121.3	C25—C26—C21	119.8 (3)
C5—C6—C7	121.2 (3)	C25—C26—H26	120.1
C5—C6—H6	119.4	C21—C26—H26	120.1
C7—C6—H6	119.4	C32—C31—C36	119.9 (2)
C6—C7—C2	120.1 (3)	C32—C31—P1	122.1 (2)
C6—C7—H7	120.0	C36—C31—P1	118.0 (2)
C2—C7—H7	120.0	C31—C32—C33	120.1 (3)
O1—C8—H8A	109.5	C31—C32—H32	120.0
O1—C8—H8B	109.5	C33—C32—H32	120.0
H8A—C8—H8B	109.5	C34—C33—C32	120.1 (3)
O1—C8—H8C	109.5	C34—C33—H33	120.0
H8A—C8—H8C	109.5	C32—C33—H33	120.0
H8B—C8—H8C	109.5	C35—C34—C33	119.8 (3)
C16—C11—C12	120.0 (3)	C35—C34—H34	120.1
C16—C11—P1	122.6 (2)	C33—C34—H34	120.1
C12—C11—P1	117.4 (2)	C34—C35—C36	120.8 (3)
C13—C12—C11	119.7 (3)	C34—C35—H35	119.6
C13—C12—H12	120.1	C36—C35—H35	119.6
C11—C12—H12	120.1	C35—C36—C31	119.4 (3)
C12—C13—C14	120.6 (3)	C35—C36—H36	120.3
C12—C13—H13	119.7	C31—C36—H36	120.3
C14—C13—H13	119.7		

C2—N1—C1—O1	−175.8 (2)	P1—C11—C16—C15	178.3 (2)
C2—N1—C1—S1	5.8 (4)	C14—C15—C16—C11	1.1 (4)
C8—O1—C1—N1	−3.5 (4)	C11—P1—C21—C26	12.2 (2)
C8—O1—C1—S1	175.15 (19)	C31—P1—C21—C26	−100.1 (2)
Au—S1—C1—N1	−157.0 (2)	Au—P1—C21—C26	137.4 (2)
Au—S1—C1—O1	24.52 (19)	C11—P1—C21—C22	−166.8 (2)
C1—N1—C2—C3	−107.2 (3)	C31—P1—C21—C22	80.9 (2)
C1—N1—C2—C7	78.0 (4)	Au—P1—C21—C22	−41.6 (2)
C7—C2—C3—C4	−0.7 (4)	C26—C21—C22—C23	0.5 (4)
N1—C2—C3—C4	−175.6 (3)	P1—C21—C22—C23	179.5 (2)

C2—C3—C4—F1	−179.1 (2)	C21—C22—C23—C24	−0.7 (5)
C2—C3—C4—C5	0.0 (4)	C22—C23—C24—C25	0.1 (5)
F1—C4—C5—C6	179.8 (3)	C23—C24—C25—C26	0.8 (4)
C3—C4—C5—C6	0.7 (5)	C24—C25—C26—C21	−1.0 (4)
C4—C5—C6—C7	−0.8 (4)	C22—C21—C26—C25	0.4 (4)
C5—C6—C7—C2	0.1 (4)	P1—C21—C26—C25	−178.6 (2)
C3—C2—C7—C6	0.6 (4)	C11—P1—C31—C32	−94.4 (3)
N1—C2—C7—C6	175.5 (3)	C21—P1—C31—C32	17.1 (3)
C21—P1—C11—C16	−109.9 (2)	Au—P1—C31—C32	139.2 (2)
C31—P1—C11—C16	2.9 (3)	C11—P1—C31—C36	86.5 (3)
Au—P1—C11—C16	127.3 (2)	C21—P1—C31—C36	−161.9 (2)
C21—P1—C11—C12	70.2 (2)	Au—P1—C31—C36	−39.9 (3)
C31—P1—C11—C12	−177.0 (2)	C36—C31—C32—C33	−1.0 (4)
Au—P1—C11—C12	−52.6 (2)	P1—C31—C32—C33	179.9 (2)
C16—C11—C12—C13	1.5 (4)	C31—C32—C33—C34	−0.2 (4)
P1—C11—C12—C13	−178.7 (2)	C32—C33—C34—C35	0.6 (5)
C11—C12—C13—C14	−0.3 (4)	C33—C34—C35—C36	0.2 (5)
C12—C13—C14—C15	−0.5 (4)	C34—C35—C36—C31	−1.3 (5)
C13—C14—C15—C16	0.1 (4)	C32—C31—C36—C35	1.8 (5)
C12—C11—C16—C15	−1.9 (4)	P1—C31—C36—C35	−179.1 (3)

Hydrogen-bond geometry (Å, º)

*Cg*1 and *Cg*2 are the centroids of the (C2–C7) and (C11–C16) rings, respectively.

D—H···*A*	*D*—H	H···*A*	*D*···*A*	*D*—H···*A*
C3—H3···O1^{i}	0.95	2.42	3.269 (3)	148
C36—H36···F1^{i}	0.95	2.51	3.218 (4)	131
C13—H13···S1^{ii}	0.95	2.83	3.519 (3)	130
C13—H13···*Cg*1^{ii}	0.95	2.74	3.500 (3)	137
C22—H22···*Cg*1^{iii}	0.95	2.63	3.397 (3)	138
C24—H24···*Cg*2^{iv}	0.95	2.80	3.552 (3)	137

Symmetry codes: (i) −*x*+1, −*y*+1, −*z*+1; (ii) −*x*+1/2, *y*−1/2, −*z*+1/2; (iii) −*x*, −*y*+1, −*z*+1; (iv) *x*−1, *y*, *z*.